Title

Experimental and Computational Investigation of Lepidocrocite Anodes for Sodium-Ion Batteries

Journal

Chemistry of Materials, 28(12)

ISSN

0897-4756

Authors

Markus, Isaac M
Engelke, Simon
Shirpour, Mona
et al.

Publication Date

2016-06-28

DOI

10.1021/acs.chemmater.6b01074

Peer reviewed

Experimental and Computational Investigation of Lepidocrocite Anodes for Sodium-Ion Batteries

Journal:	*Chemistry of Materials*
Manuscript ID	cm-2016-010744.R1
Manuscript Type:	Article
Date Submitted by the Author:	13-May-2016

Complete List of Authors:	Markus, Isaac; UC Berkeley, Material Science and Engineering Engelke, Simon; University of Cambridge Shirpour, Mona; Lawrence Berkeley National Laboratory, Environmental Energy Technologies Division Asta, Mark; University of California, Department of Materials Science and Engineering Doeff, Marca; Lawrence Berkeley National Laboratory, Materials Sciences Division

Experimental and Computational Investigation of Lepidocrocite Anodes for Sodium-Ion Batteries

Isaac M. Markus,[*,†,‡] Simon Engelke,[‡,§] Mona Shirpour,[‡,∥] Mark Asta,[*,†,¶] and Marca Doeff[‡]

Material Science and Engineering Department, University of California Berkeley, Berkeley, CA 94720, Environmental Energy Technologies Division, Lawrence Berkeley National Lab, Berkeley, CA 94720 , and Material Science Division, Lawrence Berkeley National Lab, Berkeley, CA 94720

E-mail: isaac.markus@berkeley.edu; mdasta@berkeley.edu

Abstract

In this work, we investigated several titanates with lepidocrocite-type structures (general formula $A_xTi_{1-y}M_yO_4$ with A=Na and M=Li or Mg), having potential utility as anode materials for sodium-ion batteries. First principles calculations were used to determine key battery metrics, including potential profiles, structural changes during sodiation, and sodium diffusion energy barriers for several compositions, and compared to experimental results. Site limitations were found to be critical determinants of the gravimetric capacities, which are also affected both by the stacking arrangement of the

[*]To whom correspondence should be addressed
[†]Material Science and Engineering Department, University of California Berkeley, Berkeley, CA 94720
[‡]Environmental Energy Technologies Division, Lawrence Berkeley National Lab, Berkeley, CA 94720
[¶]Material Science Division, Lawrence Berkeley National Lab, Berkeley, CA 94720
[§]Current address: Institute for Manufacturing, Department of Chemistry and Cambridge Graphene Centre, Cambridge, England
[∥]Current address: Department of Chemical Materials Engineering, University of Kentucky, Lexington, KY, USA

corrugated layers and the identity of M (Li or Mg). To explain the experimentally observed lattice parameter changes observed as a function of state-of-charge, it was necessary to assume participation of water/solvent during the sodium intercalation process. Sodium diffusion barriers were also found to vary as a function of state-of-charge and diffusion direction, with a spread of 0.06-1.3 eV at low sodium contents, narrowing to 0.3-0.5 eV at higher sodium contents. Based on these results, strategies for selecting and improving the performance of these electrode materials are suggested.

Introduction

The development of next generation systems for grid-scale energy storage projects remains one of the biggest challenges for both the modernization of the electrical grid and the integration of renewable energy sources such as solar and wind power. One main obstacle for the commercialization of such a technology is the strict cost requirement, with long term goals having to meet the benchmark set by DOE of less than \$250/kWh.[1–3] The current set of commercial battery technologies, led by high power lithium-ion batteries (LIBs), are not well suited for many of the grid storage applications, such as load leveling. This makes it an imperative to develop a broader portfolio of battery chemistries that can address the needs and scale of each application at an acceptable cost. One of the most attractive options are sodium-ion batteries (NIBs), which in addition to featuring cheap and abundant raw material inputs, offer several synergistic benefits. Among these are the ability to replace the strategic metal Cu with Al as a current collector on the negative electrode side, and the fact that sodium salt solutions are generally more conductive than the lithium analogs,[4] which has important implications for the design of cells. Another advantage of NIBs arises due to the similarity between the manufacturing and processing techniques used for LIBs, requiring less engineering development for large-scale production of such batteries compared to other types of "'Beyond-Lithium-Ion"' batteries under consideration.

Currently, among the biggest drawbacks of NIBs is the lack of a suitable negative elec-

trode.[5] While graphite can intercalate lithium and be used as the negative electrode in LIBs, it does not intercalate sodium to a significant degree. Hard carbons may be used as anodes in sodium systems,[6] but have low densities and are electroactive close to the sodium plating potential, posing safety concerns. Other candidate anode materials include Sn and Sb alloys, which exhibit rapid capacity losses with prolonged cycling due to large volume expansions during sodiation.[7] An alternative set of materials includes intercalation oxides, with layered titanates offering a rich compositional and structural range of materials that can intercalate sodium.[8–13] In this work we examine several titanates having lepidocrocite-type structures employing electrochemical testing and first-principles density-functional theory (DFT) calculations. The calculations are used to determine kinetic and thermodynamic limitations of these materials for application as anodes in NIBs. The lepidocrocite compounds are isomorphs of the mineral γ- FeOOH, and have the general formula $A_xTi_{2-y}M_yO4$ where A=K, Rb, Cs; and M = Li, Mg, Co, Fe, Ni, Cu, etc; with additional compounds possible by ion exchanging the A cation with lighter elements such as Na.[14–19] The structures form as stepped layered materials with a step size of one, with the corrugated layers either arranged in phase with one another or out of phase, corresponding to a shift of half a unit cell in the a direction. Structures with the space group $Cmcm$ (C-type) and $Pmmm$ (P-type), which are relevant to this discussion are shown in Figure 1. Although there are several other symmetries possible for lepidocrocite titanates, depending on factors such as the site occupancies in the interlayer spaces, they are not considered here. Previous experimental work on the $A_{0.8}Ti_{1.73}Li_{0.27}O_4$ (A=K, Na) system indicated that both C-type and P-type structures can be produced, depending upon the identity of A and the thermal treatment, with the highest stable cycling capacities of 150 mAh/g observed for the P-type sodiated version in unoptimized sodium half cells.[12,20] Cell performance for these systems was highly dependent on details of the electrode and materials fabrication, such as the type of binder used and post-processing steps such as carbon coating.

In the current work we employ first-principles DFT calculations with the aim of decou-

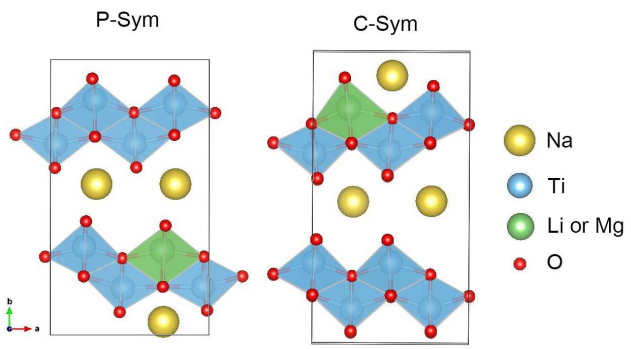

Figure 1: Sodium titanium lepidocrocite structure with P-type and C-type symmetry. The blue and green shaded polygons represent edge sharing octahedra for Ti and Li, respectively. The yellow spheres represents some of the possible sodium atoms in the pristine structure.

pling cell-engineering effects from fundamental materials properties. The first-principles calculations performed were for the materials having idealized stoichiometries of $Na_{0.75}Ti_{1.75}Li_{0.25}O_4$ for C-type and P-type phases, close to that of experimentally achieved samples; and for $Na_{1.0}Ti_{1.5}Mg_{0.5}O_4$ and $Na_{0.75}Ti_{1.625}Mg_{0.375}O_4$ having P-type symmetry, which also can be synthesized in the laboratory. Additionally, $Na_{0.75}Ti_{1.75}Mg_{0.25}O_4$ was investigated in order to enable a direct comparison of Li and Mg containing compounds with otherwise identical compositions, even though the latter has not been synthesized experimentally. The stoichiometries listed above were selected based on proximity to the ones achieved experimentally considering computational resource limitations to avoid the need for prohibitively large supercells. Simulations specifically modeled structural changes during sodiation to understand their unusually low intercalation potentials, taking into consideration the presence of interstitial water. We also present computational and experimental results for the previously mentioned Mg-containing structures in order to explore the potential applicability of other compositions with lepidocrocite structures in sodium ion batteries. The results from the latter materials compounds represent, to the best of our knowledge, the first measurements related to the performance of these materials for battery applications. The results thus provide a more comprehensive understanding of the limitations of lepidocrocite-type compounds for NIBs without complications from cell engineering effects. From these results we present design recommendations for future candidate materials for applications in NIBs.

Methods

DFT Simulations

First-principles calculations were performed using the Vienna *ab initio* simulation package (VASP), employing the Generalized Gradient Approximation (GGA) due to Perdew, Burke, and Ernzerhof (PBE).[21] The simulations were carried out using the projector augmented wave (PAW) method,[22,23] as implemented in the VASP code.[22,24] Specifically we made use of the PBE PAW potentials Na with one valence electron ($3s^1$), O with 6 valence electrons ($2s^2 2p^4$), Ti with 4 valence electrons ($3d^3 4s^1$), Li with one valence electron ($2s^1$), and Mg with two valence electrons ($3s^2$). DFT calculations made use of supercells composed of four unit cells with a plane wave energy cutoff of 500 eV, and a Γ centered k-point grid of 3x2x4. In these calculations the energy was converged to 10^{-6} eV in the self-consistent charge-density solutions, and the Hellman-Feynman forces on the ions were converged to 10 meV/Å in the structural relaxations. Calculations were spin polarized to account for the local moment of Ti^{+3} once sodium is intercalated. Additionally, the calculations employed corrections for van der Waals interactions, as well as Hubbard-U corrections for the Ti cation *d* electrons. These corrections were included after finding that they were needed to stabilize the C type symmetry at higher sodium contents, consistent with experimental findings. The van der Waals correction employed was the so-called DFT-D2 method due to Grimme as implemented in VASP.[25] Hubbard-U corrections were included employing the method due to Dudarev *et al.*,[26] with a value of U-J=4.0 eV for Ti *d* electrons, based on literature values reported for other layered titanates.[27] Calculations of electrochemical potentials were performed utilizing standard methods described in the literature.[7,28] To calculate the diffusion energy barriers the climbing-image nudge elastic band (CI-NEB) method was used.[29–33] In the CI-NEB calculations, initial and final configurations were selected from sampling sodium positions at different interstitial sites in the structure. The minimum energy paths were calculated from linear interpolation of initial and final position using at least 5 images in the CI-NEB

calculations.

Material Synthesis

The anode materials $Na_{0.7}Ti_{1.65}Mg_{0.40}O_4$, $Na_{0.9}Ti_{1.55}Mg_{0.45}O_4$ and $Na_{0.8}Ti_{1.73}Li_{0.27}O_4$ were synthesized using the solid state method by Shirpour *et al.*[12] $K_{0.7}Ti_{1.65}Mg_{0.35}O_4$, $K_{0.9}Ti_{1.55}Mg_{0.45}O_4$ and $K_{0.8}Ti_{1.73}Li_{0.27}O_4$ were prepared via the solid state reaction of MgO (purity min. 95.0%, Alfa Aesar), K_2CO_3 (purity 99.0%, Sigma-Aldrich), TiO_2 (anatase, purity 99.7%,<25 nm, Sigma-Aldrich), and Li_2CO_3 (purity 99+%, Aldrich). First, stoichiometric mixtures of the precursors were mixed in a mortar for 5 min. The mixtures were calcined in an alumina crucible at 1000^o C for 21 h in a Thermo Scientific Lindberg Blue M oven. The synthesized powder was first milled in a mortar for five minutes and the obtained phases were confirmed through X-ray powder diffraction (XRD) spectra on a Bruker X-ray Diffractometer (XRD, D2-Phaser). The materials were ranked based on crystallinity, as seen by sharp peaks for the lower angles, and the most suitable materials were milled in a planetary mill with 10 zirconia balls, each 0.5 cm diameter, at 300 rpm for 2 hours in acetone. The jar was opened after milling, the balls were removed, and the acetone was evaporated in air. The powder was collected and ground in a mortar. A 4.0 M NaCl solution was prepared and the products were each ion exchanged by stirring the powders in the solution in 200 ml flasks at 80^o C for 8 days. The resulting materials were washed with plain water to remove the salt, air dried, then dried in an oven at 50^o C and dried in a vacuum oven overnight.

Electrochemical Testing

The electrochemical properties of the compounds were evaluated in two-electrode 2032 coin cells containing metallic sodium foils as negative electrodes (half-cells). For this, bulk dry sodium (Sigma Aldrich) was extruded into thin foils and cut to size to make sodium anodes for these cells. For the positive electrodes, active material and acetylene black were first mixed together for 2 hours at 300 rpm in a planetary mill. Composite working electrodes were

prepared by making a slurry containing 70 wt% of the active material, 20−25 wt% acetylene black (Denka, 50% compressed), and 5−10 wt% polyvinylidene difluoride (PVDF) (99.5+%, Aldrich) binder in N-methyl-2-pyrrolidinone (NMP). The slurry was cast onto carbon coated aluminum foil (Exopack Advanced Coatings). The electrodes were dried first in air and then under vacuum at 120^o C for 12 hours before being cut to size and weighed in a helium filled glovebox. The typical loading and thickness were 5 mg/cm^2 and 60 μm, respectively. The electrolyte used was a solution of 1 M $NaPF_6$ (Sigma Aldrich) in ethylene carbonate/ dimethyl carbonate (EC:DMC; 3:7 mol, from Novolyte Technologies) made in house, and one or two Celgard 3401 separators were used in the coin cells. Galvanostatic cycling experiments at room temperature were carried out with a Bio-logic VMP3 potentiostat/galvanostat.

Results and Discussion

Prior to performing DFT calculations, the possible specific capacities for different lepidocrocite structures were calculated based solely on compositional and structural considerations. Figure 2 shows the relationship between composition and theoretical specific capacity for the $A_xTi_{1-y}M_yO_4$ system where M = Li^+ or Mg^{2+} and A is Li^+, Na^+ or K^+. Two scenarios are presented, one in which capacity is limited by the number of reducible Ti ions, and the other where the limitation is the number of sites available for ion insertion. (Note that not every composition shown on this graph can be synthesized; the intent is primarily to show how composition affects capacity). The site-limited case is relevant to insertion of sodium ions into the structure, because of their relatively large size. Higher capacities might be expected in the case of lithium intercalation, where A = Li^+, because of the smaller size of these ions, although it is still unlikely that the upper limit determined by the amount of reducible titanium can be achieved. From this graph, it is obvious that it is generally desirable to maximize titanium content (minimize y) and, to a lesser extent, choose lighter cations for A, no matter what the limitation. Similar considerations apply for other compo-

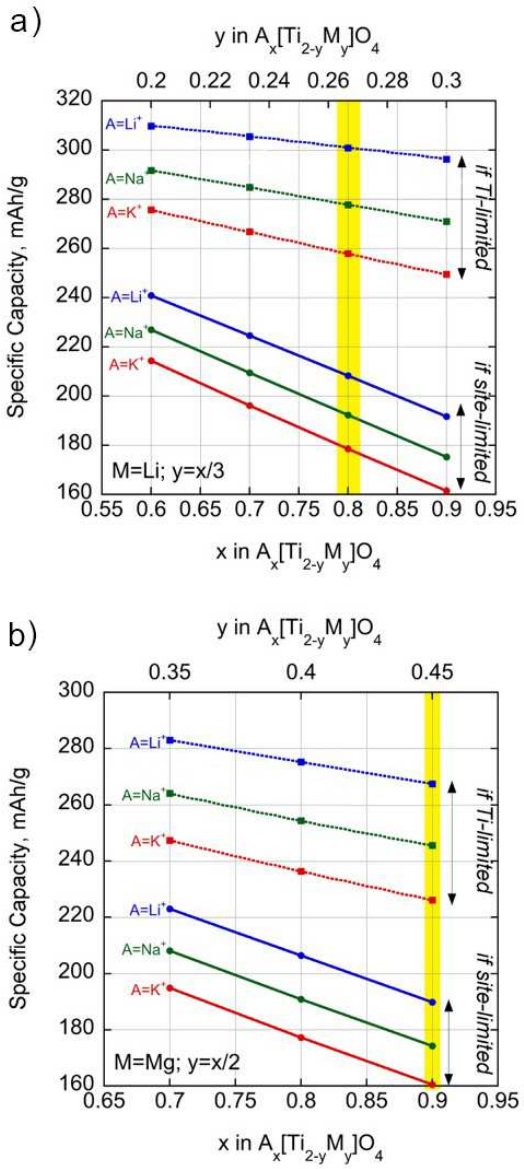

Figure 2: Theoretical calculation of gravimetric capacity for a) lithium and b) magnesium containing lepidocrocite structures with different initial stoichiometries considering situations limited by the number of Ti ions or by the number of available sites for sodium intercalation. The highlighted regions corresponds to experimentally achieved stoichiometries.

sitions (e.g., when M = Mg^{2+} and y=x/2). In practice, choices of materials are limited by the solid-solution behavior of the systems.

First-principles calculations were thus employed to provide an understanding of different experimental observations reported in the literature for distinct lepidocrocite-like compounds. Experimental results for $A_{0.8}Ti_{1.73}Li_{0.27}O_4$ (A=K, Na) electrodes have shown that

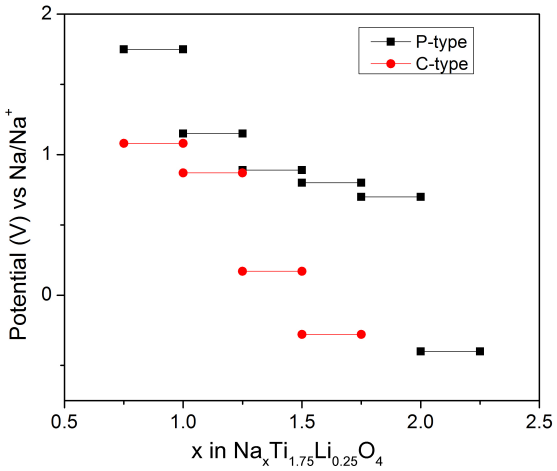

Figure 3: Calculated intercalation potential for P-type (black lines) and C-type (red lines) $Na_{0.75}Ti_{1.75}Li_{0.25}O_4$.

the P-type materials generally deliver higher practical capacities than C-type, regardless of whether A = Na^+ or K^+.[12,20] In order to understand the underlying reasons for the capacity difference we performed structural optimizations and total-energy calculations for $Na_{0.75}Ti_{1.75}Li_{0.25}O_4$ having both P-type and C-type arrangements, and calculated the potential profiles for both types of structures. As shown in Fig. 3, the P-type symmetry is calculated to have a higher intercalation potential and capacity than the C-type structure, with an additional 0.25-0.50 mols of Na per formula unit, or approximately 40-80 mAh/g, expected for the P-type structure. These results confirm that neither P-type or C-type can reach the maximum specific capacity based on reduction of all the Ti. However, the results also indicate that only the P-type structure can approach the theoretical values for site limitations shown in Figure 2a, because the C-type structure becomes less stable at higher sodium contents due to higher electrostatic repulsions between intercalated sodium ions.

Further analysis of the calculated results indicate a deviation from the experimental lattice parameters obtained during sodiation, as well as the predicted specific capacities. For an anhydrous P-type structure our calculations underestimate volume expansion by approximately 9% and overestimate the capacity by 37% (192 mAh/g vs 140 mAh/g). This discrepancy can be attributed to the model structure used in these calculations, which ignored com-

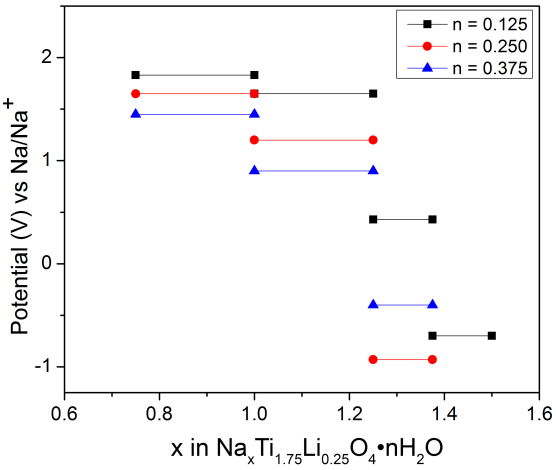

Figure 4: Calculated intercalation potential for P-type $Na_{0.75}Ti_{1.75}Li_{0.25}O_4$n H_2O , where n=0.125-0.375.

plications from a cooperative solvent co-insertion mechanism observed by Shirpour *et al.*[12] Evidence from ex-situ X-ray diffraction experiments performed on P-type $Na_{0.8}Ti_{1.73}Li_{0.27}O_4$ indicated that neutral species (water or solvent) were de-inserted concomitant with sodium intercalation during discharge, with the reverse process occurring during charge. For the portion of the electrode that was anhydrous, there was an expansion along the *b* lattice parameter during sodiation, with additional expansion occurring during the desodiation. The fully sodiated products of both the hydrated and anhydrous portion of the electrodes were identical.

To investigate the impact of interstitial water on capacity and structural changes we further refined our calculations by modeling the P-type structure including interstitial water according to $Na_{0.75}Ti_{1.75}Li_{0.25}O_4$ •nH_2O with n ranging from 0.125-1.25 mols. The results shown in Figure 4, indicate that the predicted capacity of the material decreases with increasing solvent content, as there are fewer electrostatically stable sites for sodium insertion. However, this is only true if the neutral species are not displaced by sodium during discharge. The cooperative displacement mechanism is unlikely to be completely efficient, presenting one possibility for the discrepancies found between the experimental and computational results for the capacity, because theoretically this material should be able to accommodate

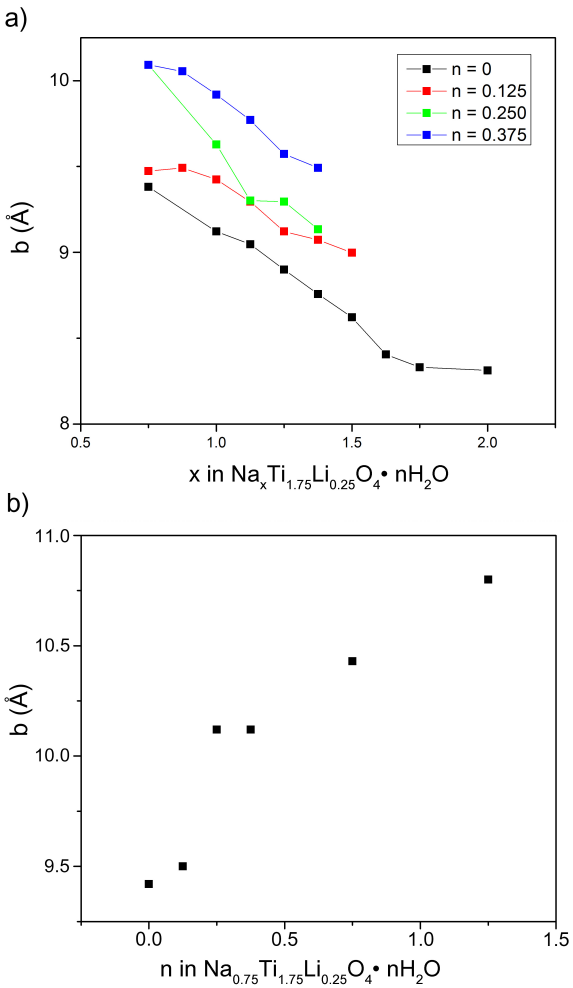

Figure 5: Shows the computationally derived change in the b lattice parameters with increasing sodium concentration for the P-type lepidocrocite with water content ranging from 0-0.375. b) shows the change in the b lattice parameter for $Na_{0.75}Ti_{1.75}Li_{0.25}O_4 \bullet nH_2O$ with water content increasing from n= 0 to n= 1.5.

more sodium intercalation than is observed in the actual half-cell experiments.

Further evidence that the material is susceptible to a cooperative solvent uptake is obtained by analyzing the changes to the lattice parameters during sodiation. Figure 5a, shows the changes to the b lattice parameter during sodiation for P-type lepidocrocite titanates with water content ranging from n = 0 to 0.375 mols per formula unit. As can be seen the b lattice parameter contracts during sodium insertion, following similar behavior to the experimental results for the solvated samples. For comparison, the b lattice parameter is also plotted in Fig. 5b for the same P-type lepidocrocite given a fixed sodium concentration with increas-

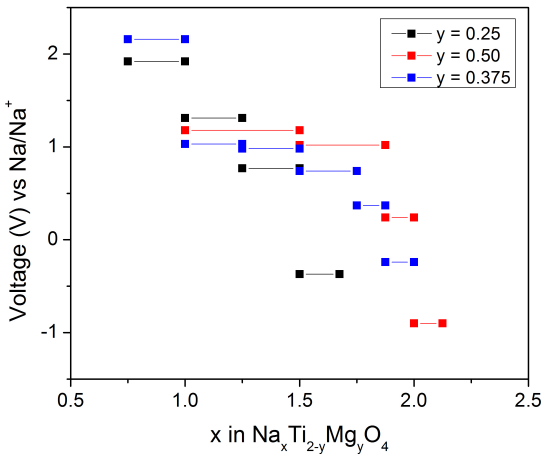

Figure 6: Calculated intercalation potential for P P-type (blue lines) $Na_{0.75}Ti_{1.75}Mg_{0.25}O_4$.

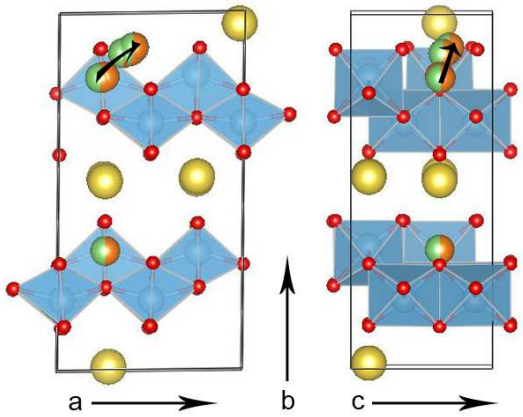

Figure 7: Lithium or magnesium diffusion minimum energy path for diffusion from Ti site to sodium site.

ing water content from n = 0 to 1.25 mols per formula unit. The results shows a steady increase in the lattice parameter upon desodiation similar to that found experimentally for the dehydrated sample. These results support the conclusion that sodium ions and solvent molecules interchange during cycling. In the previous work by Shirpour *et al.*[12] interlayer charge density was established as an important parameter for predicting such behavior, and given that the results obtained herein are consistent, future material selection and testing should consider this susceptibility to solvent uptake as a possible reason for materials failing to deliver their theoretical capacities.

In order to further understand the sodium intercalation mechanism in lepidocrocite-type

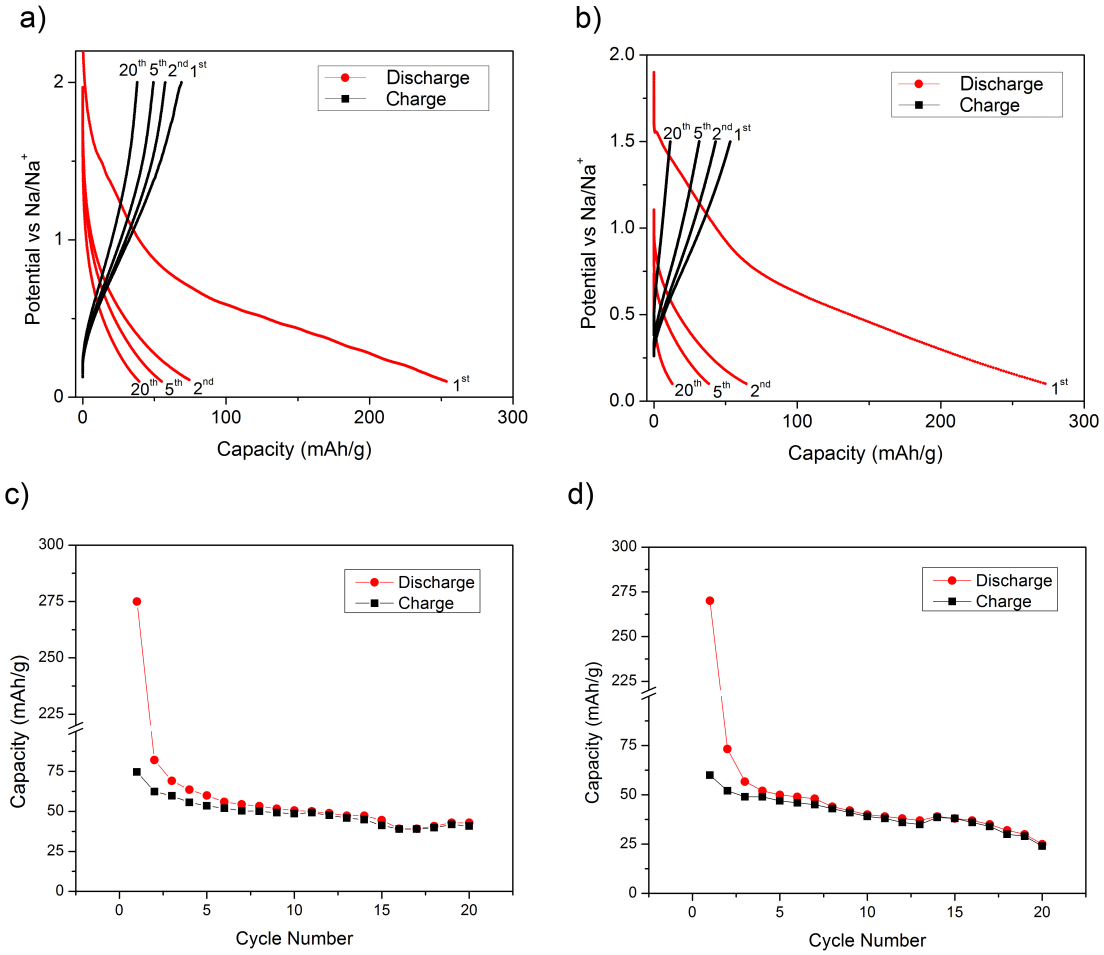

Figure 8: a,b) Show select discharge and charge capacity curves for (a) $Na_{0.7}Ti_{1.45}Mg_{0.35}O_4$ and (b) $Na_{0.9}Ti_{1.55}Mg_{0.45}O_4$. Parts c,d) show the discharge and charge capacity for (c) $Na_{0.7}Ti_{1.45}Mg_{0.35}O_4$ and (d) $Na_{0.9}Ti_{1.55}Mg_{0.45}O_4$ for 20 cycles. The cells were cycled in Na half cells between 2.5 and 0.1 V at 0.06 to 0.08 mA cm^{-2} (20 mAg^{-1})

titanates, DFT calculations and experiments were performed with Mg containing structures. Calculations were performed on the compounds $Na_{0.75}Ti_{1.625}Mg_{0.375}O_4$, $Na_{1.0}Ti_{1.50}Mg_{0.50}O_4$, and a hypothetical composition of $Na_{0.75}Ti_{1.75}Mg_{0.25}O_4$ with P-type structures. The latter material was selected to be able to directly compare results with the Li containing analog discussed above, although it cannot be prepared directly by solid-state synthesis methods.[16] Results for the intercalation potential of each structure are shown in Fig. 6, with the $Na_{0.75}Ti_{1.625}Mg_{0.375}O_4$ stoichiometry predicted to have the highest capacity of the three compositions examined. All of the Mg-containing structures have lower predicted capacities

than those determined for the P-type Li containing compound. By calculating the structural changes for both lithium and magnesium containing compounds with the same stoichiometry, we found that at higher sodium contents, the lithium is predicted to drop from octahedral positions in the metal oxide layer into adjacent tetrahedral positions. An analogous process is not predicted to occur for the magnesium containing compound (i.e., Mg is predicted to be less mobile). Employing nudge elastic band calculations we found that lithium has a 0.29 eV energy barrier to jump from the titanium 4c site to a vacant sodium 8a site in the C-type lepidocrocite, while in the P-type structure lithium had an energy barrier of 0.42 eV and magnesium had an energy barrier of 0.71 eV. Because the lithium ions have energy barriers comparable to those calculated for intercalating sodium, it is likely they can diffuse out of their sites in the transition metal layer during either the ion exchange process or the sodiation process that occurs upon cycling. From a practical perspective, the differences in energy barriers suggest that the greater lithium mobility can facilitate higher sodium insertion by enabling Li to leave its initial site in the host structure during discharge, thus reducing internal stress and electrostatic interactions between sodium.

The lower capacity predicted for magnesium substituted materials was verified experimentally by synthesizing two different compositions, $Na_{0.9}Ti_{1.55}Mg_{0.45}O_4$ and $Na_{0.7}Ti_{1.65}Mg_{0.35}O_4$, and testing them in a Na half cell. The XRD patterns for the two compositions are shown in Fig. 3S in the supplemental information; the results are consistent with nearly phase-pure lepidocrocite structures, with small traces of impurities arising from the ion-exchange process. Fig. 8 shows electrochemical cycling data for both compositions. With the exception of the first cycle discharge capacity, both tested compositions achieved lower capacities than those previously reported by Shirpour *et al.*[12] for the Li containing lepidocrocite titanate. Due to the low potentials at which these compounds discharge, side reactions due to irreversible reduction of electrolyte and formation of a solid electrolyte interface (SEI) contribute capacity to the first discharge. The second discharge is therefore a more accurate reflection of the true capacities of these materials. Given that the material synthesis, cell fabrication,

and testing were comparable for the two types of materials, this verifies the information presented in Figure 6, that the Mg-containing titanates will have lower capacities than the Li-containing one. This is significant particularly for the $Na_{0.7}Ti_{1.65}Mg_{0.35}O_4$ composition, because the titanium content is nearly the same as that of $Na_{0.8}Ti_{1.73}Li_{0.27}O_4$ and there should be fewer site limitations due to the lower sodium content in the pristine material.

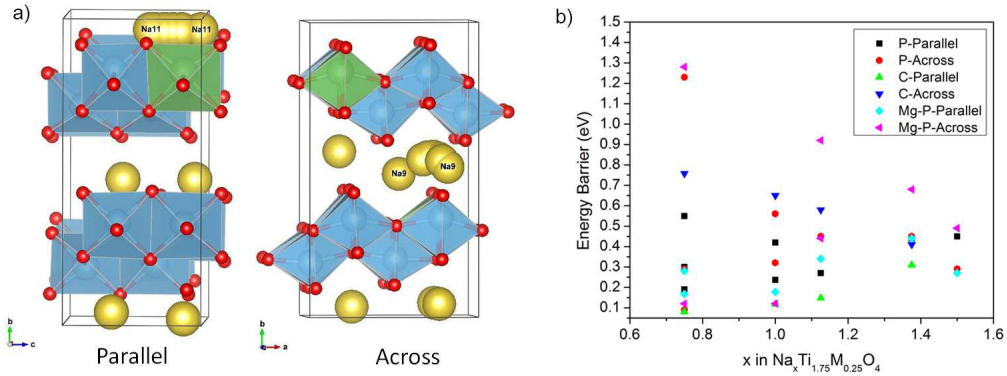

Figure 9: a) Shows the two types of minimum energy paths consider for sodium diffusion, parallel refers to sodium movement along corrugation in the c direction, and across refers to sodium diffusion perpendicular to corrugation along the a direction. b) Shows the energy barriers for sodium diffusion at different sodium concentration for the the P-type and C-type lithium substituted phases, and the P-type magnesium substituted phase.

Lastly, we examined the energy barriers for sodium diffusion in the P-type and C-type structures containing lithium and the P-type structure containing Mg with the stoichiometry $Na_{0.75}Ti_{1.75}Mg_{0.25}O_4$. Energy barriers were calculated parallel to the corrugation along the a lattice direction and perpendicular to the corrugations along the c direction for the different configurations available at each sodium concentration. Fig. 9b shows that the P-type and C-type structures exhibit slightly different behaviors that translate to different cycling properties. The calculated values for different sodium concentrations in the P-type structure reveal a wide spread at lower concentrations that narrows with increasing sodium content. The results suggest that there is a strong correlation for sodium diffusion with electrostatic repulsion from other sodium cations, since the larger energy barriers are generated when there are non-diffusing sodium cations nearby. This implies that the P-type materials have strong kinetic dependences on the state-of-charge, regardless of the identity of the substituent (Li

or Mg). Furthermore, analysis of the spread of energy barriers for each phase reveals possible dependence on the charge/discharge rates. For the P-type material, the availability of more interstitial sites with different local electrostatic environments results in a broader spread of diffusion paths for either across or parallel jump types. Because the low energy barrier paths are only accessible when the sodium ions are spread out more homogeneously, fast current rates can result in the formation of local concentration gradients that force sodium to diffuse across higher energy paths. Evidence supporting this hypothesis is provided in Figure 10, which shows electrochemical cycling of Na half cells with the material $Na_{0.8}Ti_{1.73}Li0.27O_4$ employing different current rates. This material was synthesized and tested previously by Shirpour *et al.*[12] The data indicates that cells cycled with currents rates of 0.2 mA/cm^2 (67.5 mA/g) deliver less than half the capacity than cells with 0.04 mA/cm^2 (13.5 mA/g). The slower current rate allows the material to deliver initial higher capacities that permit a higher number cycles before delivering equal discharge capacities.

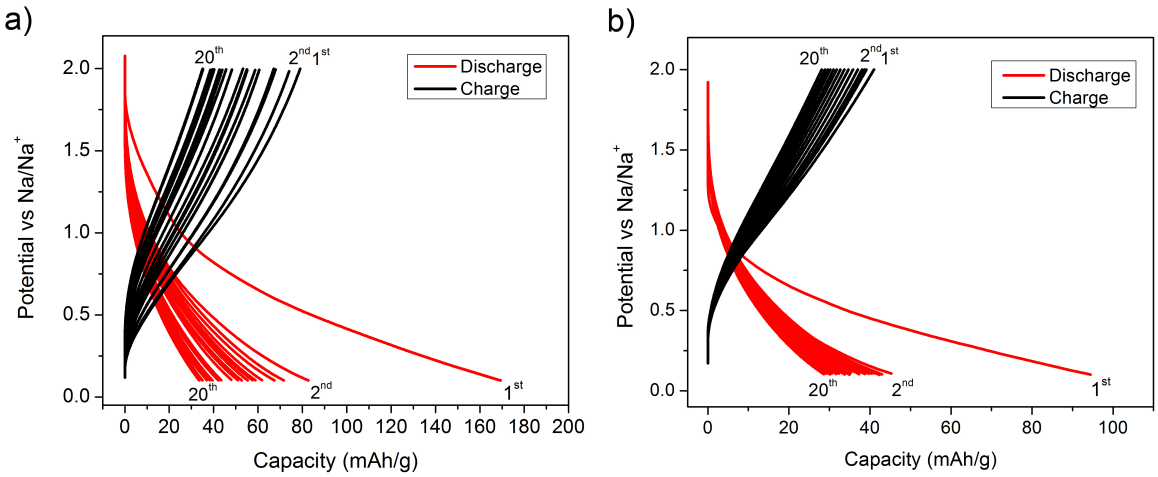

Figure 10: Specific capacity for $Na_{0.8}Ti_{1.73}Li_{0.27}O_4$ Na half cells with currents rates of (a) 0.04 mA/cm^2 and (b) 0.2 mA/cm^2 .

In these structures as the sodium content increases and the material becomes more electrostatically homogenous, there is less variance in the energy barriers with the direction, with an average value of 0.4 eV predicted for these materials when standard electrode slurries are used to fabricate cells. However, the lowest energy barriers were available for parallel

diffusion when there were no other sodium ions nearby suggesting that the material would exhibit anisotropic conduction similar to 1D diffusion materials. This is predicted to be the case for the C-type structure, which as can be seen in Fig. 9b does not have the spread in energy barriers that the P-type material does. Because this material has fewer symmetrically distinct sites for Na intercalation, its diffusion paths are more clearly defined with noticeable anisotropic behavior. The bright green and dark blue triangles indicate diffusion barriers that are parallel or across the corrugation, respectively. As can be seen the barriers follow almost linear behavior with the sodium content, suggesting state-of-charge is also important for this phase. However, from these results it appears that fast 1-dimensional diffusion is possible parallel to the corrugations, with energy barriers ranging from 0.06 to 0.3 eV. This suggest that this phase could have superior rate capability to the P-type structures. Evidence for this finding has been reported by Chen et. al,[20] who found that in the C-type material $K_{0.8}Ti_{1.73}Li_{0.27}O_4$ that has been ball milled and carbon coated, the capacity decreases from 110 mAh/g to 60 mAh/g when increasing the current from 20 mA/g to 200 mA/g, with full capacity recovery when current is decreased back to 20 mA/g. Superior performance is also reported in work by Katogi et al.,[34] which shows that the C-centered lepidocrocite $Na_{0.9}Ti_{1.7}Li_{0.3}O_4$ has excellent rate capability, with over 80% capacity retention when increasing the current from C/17.5 to 10C.

The combined computational and experimental results indicate that future work on lepidocrocite type materials need to consider application requirements. Although Li substituted P-type structures are predicted to have higher capacities, it is the C-type materials that are expected to have good rate capabilities. Taking advantage of potentially fast 1-dimensional diffusion requires that particle size be optimized in order to limit kinetic effects because any blockage of diffusion channels could severely impact performance or rate capability for these materials. Furthermore, given that site limitations create an upper boundary for the amount of sodium that can be intercalated, different strategies such as aliovalent ion substitution or interlayer spacing engineering, should be consider to increase the practical capacity of these

materials.

Conclusions

Using first-principles calculations coupled with experimental measurements, we have explored several properties of the lepidocrocite-structured titanates as a function of composition and stacking arrangement. Intercalation potential calculations revealed that the capacities of these materials are limited by site limitations and electrostatic considerations rather than the number of redox active centers. Based on structural considerations, the highest practical capacity should be achieved for the P-type $Na_{0.75}Ti_{1.75}Li_{0.25}O_4$ material, corresponding to insertion of $\sim$1.25 mols of sodium per formula unit. When effects from interstitial water are included, it appears that practical capacity is decreased due to solvent uptake. This reduces site availability for sodium intercalation in the experimental setup. A positive effect previously observed and corroborated by structural relaxation calculations was that this solvent-exchange mechanism is likely cooperative, reducing overall volume changes during cycling as lattice contraction along the b direction is ameliorated by concomitant solvent insertion.

A comparison between materials containing Li and Mg in the transition metal layers indicates that the former should have superior capacity because of the mobility of lithium ions, which can move out of the transition metal sites into sodium sites and relax strain. Calculations of the energy barriers for sodium diffusion indicate that the P-type structures can be rate-limited due to strong electrostatic interactions between intercalated sodium ions. The calculated energy barriers ranged from 0.1 eV to 1.3 eV before sodium intercalation and narrowed to 0.3 eV to 0.5 eV after 0.75 mols/f.u. of sodium had been intercalated. However, lower energy barriers (0.06 to 0.3 eV) were predicted for the C-type structure, with possible fast diffusion along channels parallel to the corrugations that would result in rate capability superior to that of the P-type structure. The combined findings suggest that these materials

can benefit from smaller particle sizes that can facilitate diffusion along fast channels that can reduce large concentration gradients and make fully accessible fast 1D pathways.

Acknowledgment

This work was supported by the Assistant Secretary for Energy Efficiency and Renewable Energy, Office of Vehicle Technologies of the U.S. Department of Energy under contract no. DE-AC02-05CH11231. This work made use of computational resources provided by the Extreme Science and Engineering Discovery Environment (XSEDE), which is supported by National Science Foundation under grant number ACI-1053575. I.M.M acknowledges the support of the NSF graduate research fellowship program.

References

(1) Armand, M.; Tarascon, J.-M. Building Better Batteries. *Nature* **2008**, *451*, 652–657.

(2) Gyuk, I.; Johnson, M.; Vetrano, J.; Lynn, K.; Parks, W.; Handa, R.; Kannberg, L.; Hearne, S.; Waldrip, K.; R, B. Grid Energy Storage. **2013**, 1–67.

(3) Yang, Z.; Zhang, J.; Kintner-meyer, M.; Lu, X.; Choi, D.; Lemmon, J. P. Electrochemical Energy Storage for Green Grid. *Chem. Rev.* **2011**, *111*, 3577–3613.

(4) Palomares, V.; Serras, P.; Villaluenga, I.; Hueso, K. B.; Carretero-González, J.; Rojo, T. Na-ion Batteries, Recent Advances and Present Challenges to Become Low Cost Energy Storage Systems. *Energy Environ. Sci.* **2012**, *5*, 5884.

(5) Chevrier, V. L.; Ceder, G. Challenges for Na-ion Negative Electrodes. *J. Electrochem. Soc.* **2011**, *158*, 1011–1014.

(6) Stevens, D. a.; Dahn, J. R. High Capacity Anode Materials for Rechargeable Sodium-Ion Batteries. *J. Electrochem. Soc.* **2000**, *147*, 1271.

(7) Islam, M. S.; Fisher, C. A. J. Lithium and Sodium Battery Cathode Materials: Computational Insights Into Voltage, Diffusion and Nanostructural properties. *Chem. Soc. Rev.* **2014**, *43*, 185–204.

(8) Rudola, A.; Saravanan, K.; Mason, C. W.; Balaya, P. $Na_2Ti_3O_7$: An Intercalation Based Anode for Sodium-ion Battery Applications. *J. Mater. Chem. A* **2013**, *1*, 2653.

(9) Guo, S.; Yu, H.; Liu, P.; Ren, Y.; Zhang, T.; Chen, M.; Ishida, M.; Zhou, H. High-performance Symmetric Sodium-ion Batteries Using a New, Bipolar O3-type Material, $Na_{0.8}Ni_{0.4}Ti_{0.6}O_2$. *Energy Environ. Sci.* **2015**, *8*, 1237–1244.

(10) Arrouvel, C.; Parker, S. C.; Islam, M. S. Lithium Insertion and Transport in the TiO_2-β Anode Material: A Computational Study. *Chem. Mater.* **2009**, *21*, 4778–4783.

(11) Shirpour, M.; Cabana, J.; Doeff, M. New Materials Based on a Layered Sodium Titanate for Dual Electrochemical Na and Li Intercalation Systems. *Energy Environ. Sci.* **2013**, *6*, 2538.

(12) Shirpour, M.; Cabana, J.; Doeff, M. Lepidocrocite-type Layered Titanate Structures: New Lithium and Sodium Ion Intercalation Anode Materials. *Chemistry of Materials* **2014**, *26*, 2502–2512.

(13) Senguttuvan, P.; Palacín, M. R. $Na_2Ti_3O_7$: Lowest Voltage Ever Reported Oxide Insertion Electrode for Sodium Ion Batteries. **2011**, 4109–4111.

(14) Sasaki, T.; Kooli, F.; Iida, M.; Michiue, Y.; Takenouchi, S.; Yajima, Y.; Izumi, F.; Chakoumakos, B. C.; Watanabe, M. A Mixed Alkali Metal Titanate with the Lepidocrocite-like Layered Structure. Preparation, Crystal Structure, Protonic Form, and Acid-Base Intercalation Properties. *Chem. Mater.* **1998**, *10*, 4123–4128.

(15) Gao, T.; Fjellvag, H.; Norby, P. Protonic Titanate Derived from $Cs_xTi_{2-x/2}Mg_{x/2}O_4$ (x = 0.7) with Lepidocrocite-type Layered Structure. *J. Mater. Chem.* **2009**, *19*, 787–794.

(16) Groult, D.; Mercey, C.; Raveau, B. Nouveaux Oxydes *à* Structure en Feuillets: Les Titanates de Potassium non-stoechiométriques $K_xM_yTi_{2-y}O_4$. *Journal of Solid State Chemistry* **1980**, *32*, 289 – 296.

(17) Reid, A. F.; Mumme, W. G.; Wadsley, A. D. A New Class of Compound $M_x^+A_x^{3+}Ti_{2-x}O_4$ ($0.60 < x < 0.80$) Typified by $Rb_xMn_xTi_{2-x}O_4$. *Acta Crystallogr. Sect. B Struct. Crystallogr. Cryst. Chem.* **1968**, *24*, 1228–1233.

(18) Sasaki, T.; Watanabe, M.; Michiue, Y.; Komatsu, Y.; Izumi, F.; Takenouchi, S. Preparation and Acid-Base Properties of a Protonated Titanate with the Lepidocrocite-like Layer Structure. *Chemistry of Materials* **1995**, *7*, 1001–1007.

(19) England, W.; Goodenough, J.; Wiseman, P. Ion-exchange Reactions of Mixed Oxides. *Journal of Solid State Chemistry* **1983**, *49*, 289 – 299.

(20) Chen, K.-y.; Zhang, W.-x.; Liu, Y.; Zhu, H.-p.; Duan, J.; Xiang, X.-h.; Xue, L.-h.; Huang, Y.-h. Carbon Coated $K_{0.8}Ti_{1.73}Li_{0.27}O_4$: A Novel Anode Material for Sodium-ion Batteries with a Long Cycle Life. *Chem. Commun. (Camb).* **2015**, *51*, 1608–11.

(21) Perdew, J. P.; Burke, K.; Ernzerhof, M. Generalized Gradient Approximation Made Simple. *Phys. Rev. Lett.* **1996**, *77*, 3865–3868.

(22) Kresse, G.; Joubert, D. From Ultrasoft Pseudopotentials to the Projector Augmented-wave Method. *Phys. Rev. B* **1999**, *59*, 1758–1775.

(23) Blöchl, P. E. Projector Augmented-wave Method. *Phys. Rev. B* **1994**, *50*, 17953–17979.

(24) Kresse, G.; Furthmüller, J. Efficient Iterative Schemes for *ab initio* Total-energy Calculations Using a Plane-wave Basis Set. *Phys. Rev. B* **1996**, *54*, 11169–11186.

(25) Grimme, S. Semiempirical GGA-type density functional constructed with a long-range dispersion correction. *Journal of Computational Chemistry* **2006**, *27*, 1787–1799.

(26) Dudarev, S. L.; Botton, G. A.; Savrasov, S. Y.; Humphreys, C. J.; Sutton, A. P. Electron-energy-loss Spectra and the Structural Stability of Nickel Oxide: An LSDA+U Study. *Phys. Rev. B* **1998**, *57*, 1505–1509.

(27) Morgan, B. J.; Watson, G. W. GGA + U Description of Lithium Intercalation into Anatase TiO_2. *Phys. Rev. B* **2010**, *82*, 144119.

(28) Meng, Y. S.; Arroyo-de Dompablo, M. E. First Principles Computational Materials Design for Energy Storage Materials in Lithium-ion Batteries. *Energy Environ. Sci.* **2009**, *2*, 589.

(29) Sheppard, D.; Xiao, P.; Chemelewski, W.; Johnson, D. D.; Henkelman, G. A Generalized Solid-state Nudged Elastic Band Method. *The Journal of Chemical Physics* **2012**, *136*, 074103.

(30) Sheppard, D.; Henkelman, G. Paths to Which the Nudged Elastic Band Converges. *Journal of Computational Chemistry* **2011**, *32*, 1769–1771.

(31) Sheppard, D.; Terrell, R.; Henkelman, G. Optimization Methods for Finding Minimum Energy Paths. *The Journal of Chemical Physics* **2008**, *128*, 134106.

(32) Henkelman, G.; Uberuaga, B. P.; Jónsson, H. A Climbing Image Nudged Elastic Band Method for Finding Saddle Points and Minimum Energy Paths. *The Journal of Chemical Physics* **2000**, *113*, 9901–9904.

(33) Henkelman, G.; Jónsson, H. Improved Tangent Estimate in the Nudged Elastic Band Method for Finding Minimum Energy Paths and Saddle Points. *The Journal of Chemical Physics* **2000**, *113*, 9978–9985.

(34) Katogi, A.; Kubota, A.; Miyamoto, K.; Chihara, K.; Hasegawa, T.; Komaba, S. Electrochemical Performance of C-Centered Lepidocrocite-Type Titanate for Na-Ion Battery. 18th International Meeting on Lithium Batteries (June 19-24, 2016). 2016.

Graphical TOC Entry